Symbiosis

www.symbiosisonlinepublishing.com
ISSN Online: 2374-8362

Research Article Journal of Advanced Research in Biotechnology Open Access

On similarity of specific heat capacity and capillary pressure fractal dimensions for characterizing Shajara Reservoirs of the Permo-Carboniferous Shajara Formation, Saudi Arabia

Khalid Elyas Mohamed Elameen Alkhidir*

Department of Petroleum and Natural Gas Engineering, College of Engineering, King Saud University, Saudi Arabia

Received: June 26, 2019; Accepted: July 11, 2019; Published: August 21, 2019

***Corresponding author:** Prof. Khalid Elyas Mohamed Elameen Alkhidir Ph.D., Department of Petroleum and Natural Gas Engineering, College of Engineering, King Saud University, Saudi Arabia; E-mail id: kalkhidir@ksu.edu.sa*

Abstract

The quality and assessment of a reservoir can be documented in details by the application of Specific heat capacity. This research aims to calculate fractal dimension from the relationship among Specific heat capacity, maximum Specific heat capacity and wetting phase saturation and to approve it by the fractal dimension derived from the relationship among capillary pressure and wetting phase saturation. Two equations for calculating the fractal dimensions have been employed. The first one describes the functional relationship between wetting phase saturation, Specific heat capacity, maximum Specific heat capacity and fractal dimension. The second equation implies to the wetting phase saturation as a function of capillary pressure and the fractal dimension. Two procedures for obtaining the fractal dimension have been utilized. The first procedure was done by plotting the logarithm of the ratio between Specific heat capacity and maximum Specific heat capacity versus logarithm wetting phase saturation. The slope of the first procedure = 3- DF (fractal dimension). The second procedure for obtaining the fractal dimension was determined by plotting the logarithm of capillary pressure versus the logarithm of wetting phase saturation. The slope of the second procedure = DF -3. On the basis of the obtained results of the fabricated stratigraphic column and the attained values of the fractal dimension, the sandstones of the Shajara reservoirs of the Shajara Formation were divided here into three units.

Keywords: Shajara Reservoirs; Shajara Formation; Specific Heat Capacity Fractal Dimension; Capillary Pressure Fractal Dimension

Introduction

Seismo electric effects related to electro kinetic potential, dielectric permittivity, pressure gradient, fluid viscosity, and electric conductivity was first reported by [1]. Capillary pressure follows the scaling law at low wetting phase saturation was reported by [2]. Seismo electric phenomenon by considering electro kinetic coupling coefficient as a function of effective charge density, permeability, fluid viscosity and electric conductivity was reported by [3]. The magnitude of seismo electric current depends on porosity, pore size, zeta potential of the pore surfaces, and elastic properties of the matrix was investigated by [4]. The tangent of the ratio of converted electic field to pressure is approximately in inverse proportion to permeability was studied by [5]. Permeability inversion from seismo electric log at low frequency was studied by [6]. They reported that, the tangent of the ratio among electric excitation intensity and pressure field is a function of porosity, fluid viscosity, frequency, tortuosity, and fluid density and Dracy permeability. A decrease of seismo electric frequencies with increasing water content was reported by [7]. An increase of seismo electric transfer function with increasing water saturation was studied by [8]. An increase of dynamic seismo electric transfer function with decreasing fluid conductivity was described by [9]. The amplitude of seismo electric signal increases with increasing permeability which means that the seismo electric effects are directly related to the permeability and can be used to study the permeability of the reservoir was illustrated by [10]. Seismo electric coupling is frequency dependent and decreases expontialy when frequency increases was demonstrated by [11]. An increase of permeability with increasing pressure head and bubble pressure fractal dimension was reported by [12, 13]. An increase of geometric relaxation time of induced polarization fractal dimension with permeability increasing and grain size was described by [14, 15].

Materials and Methods

Sandstone samples were collected from the surface type section of the Permo-Carboniferous Shajara Formation, latitude 26° 52’ 17.4”, longitude 43° 36’ 18”. (Figure1). Porosity was measured on collected samples using mercury intrusion Porosimetry and permeability was derived from capillary pressure data. The purpose of this paper is to obtain Specific heat capacity fractal dimension and to confirm it by capillary pressure fractal dimension. The fractal dimension of the first procedure is determined from the positive slope of the plot of logarithm of the ratio of Specific heat capacity to maximum Specific heat capacity log ($SHC^{1/2}/SHC^{1/2max}$) versus log wetting phase saturation (logSw). Whereas the fractal dimension of the second procedure is determined from the negative slope of the plot of logarithm of capillary pressure (log Pc) versus logarithm of wetting phase saturation (log Sw).

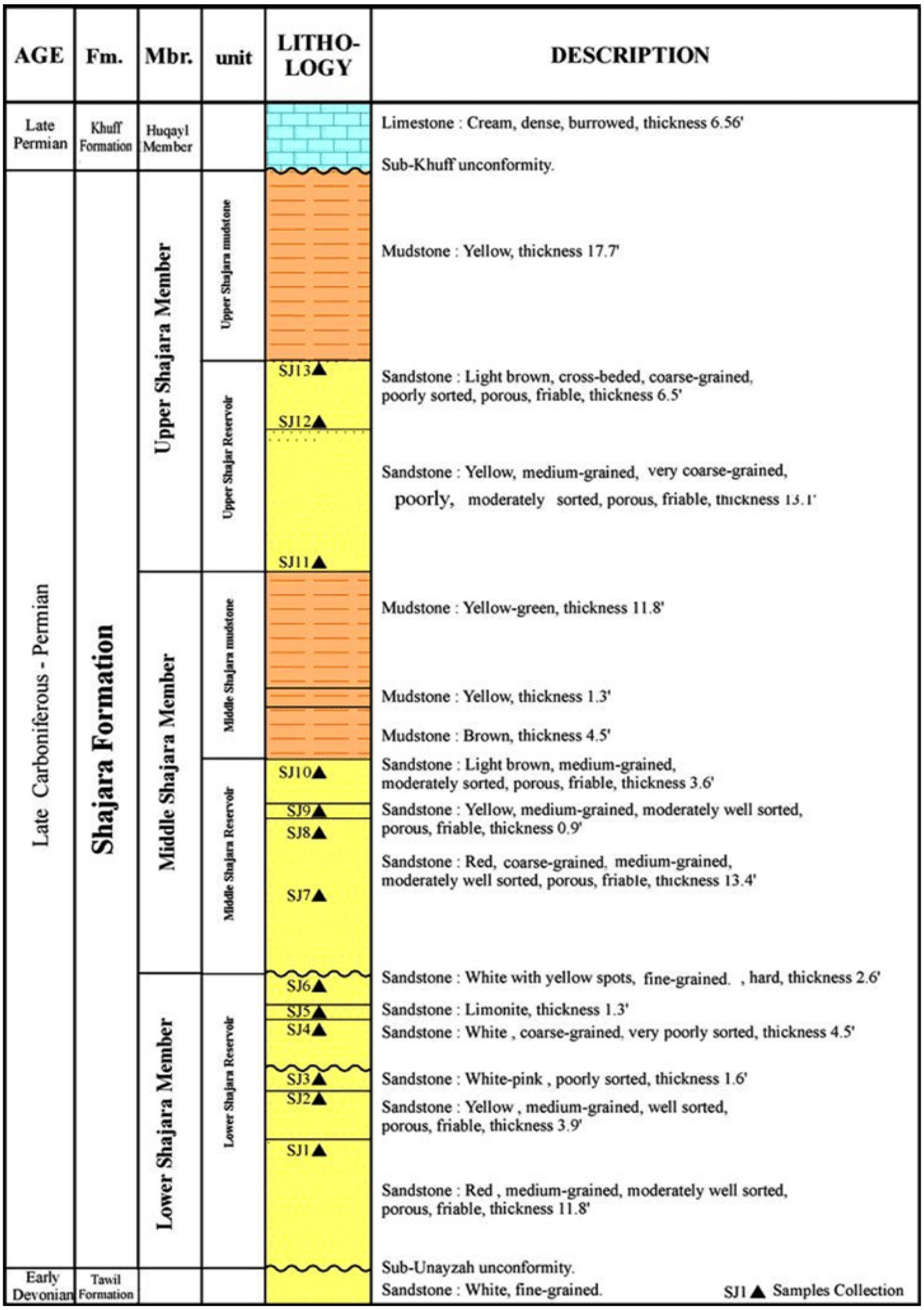

Figure 1: Surface type section of the Shajara Reservoirs of the Permo-Carboniferous Shajara Formation at latitude 26° 52’ 17.4” longitude 43° 36’ 18”

The specific heat capacity can be scaled as

$$S_w = \left[\frac{SHC^{\frac{1}{2}}}{SHC_{max}^{\frac{1}{2}}}\right]^{[3-Df]} \quad [1]$$

Where Sw the water saturation, SHC the specific heat capacity in Joule / Kelvin * kilo gram, SHC_{max} the maximum specific heat capacity in Joule / Kelvin * kilo gram, and DF the fractal dimension. Equation 1 can be proofed from

$$Q = \Delta T * m * SHC \quad [2]$$

Where Q the heat in Joule, ΔT temperature difference in Kelvin, m the mass in kilo gram, SHC the specific heat capacity in Joule / Kelvin * kilo gram. The mass m can be scaled as

$$m = \left[\frac{F}{g}\right] \quad [3]$$

Where m the mass in kilo gram, F the force in Newton, g acceleration in meter / square second Insert equation 3into equation 2

$$Q = \left[\frac{\Delta T * F * SHC}{g}\right] \quad [4]$$

The acceleration g can be scaled as

$$g = \left[\frac{E}{\Psi}\right] \quad [5]$$

Where g the acceleration in meter / square second, E the electric field in volt / meter, ψ the electric transfer function in volt * square second / square meter. Insert equation 5 into equation 4

$$Q = \left[\frac{\Delta T * F * SHC * \Psi}{E}\right] \quad [6]$$

The electric field E can be scaled as

$$E = \left[\frac{V}{CEK}\right] \quad [7]$$

Where E the electric field in volt / meter, V the velocity in meter / second, CEK the electro kinetic coefficient in ampere / pascal * meter. Insert equation 7 into equation 6

$$Q = \left[\frac{\Delta T * F * SHC * \Psi * CEK}{V}\right] \quad [8]$$

The velocity V can be scaled as

$$V = \left[\frac{Q'}{A}\right] \quad [9]$$

Where V the velocity in meter / second, Q' the flow rate in cubic meter / second, A the area in square meter Insert equation 9 into equation 8

$$Q = \left[\frac{\Delta T * F * SHC * \Psi * CEK * A}{Q'}\right] \quad [10]$$

Equation 10 after rearrange will become

$$Q * Q' = \Delta T * F * SHC * \Psi * CEK * A \quad [11]$$

The flow rate Q' can be scaled as

$$Q' = \left[\frac{k * A * \Delta P}{\mu * L}\right] \quad [12]$$

Where Q' the flow rate in cubic meter / second, k the permeability in square meter, A the area in square meter, ΔP the differential pressure in Pascal, μ the fluid viscosity in Pascal second, L the capillary length in meter. Insert equation 12 into equation 11

$$Q * k * A * \Delta P = \Delta T * F * SHC * \Psi * CEK * A * \mu * L \quad [13]$$

The maximum permeability k_{max} can be scaled as

$$Q * k_{max} * A * \Delta P = \Delta T * F * SHC_{max} * \psi * CEK * A * \mu * L \quad [14]$$

Divide equation 13 by equation 14

$$\left[\frac{Q * k * A * \Delta P}{Q * k_{max} * A * \Delta P}\right] = \left[\frac{\Delta T * F * SHC * \psi * CEK * A * \mu * L}{\Delta T * F * SHC_{max} * \psi * CEK * A * \mu * L}\right] \quad [15]$$

Equation 15 after simplification will become

$$\left[\frac{k}{k_{max}}\right] = \left[\frac{SHC}{SHC_{max}}\right] \quad [16]$$

Take the square root of equation 16

$$\sqrt{\left[\frac{k}{k_{max}}\right]} \quad \sqrt{\left[\frac{SHC}{SHC_{max}}\right]} \quad [17]$$

Equation 17 after simplification will become

$$\left[\frac{k^{\frac{1}{2}}}{k_{max}^{\frac{1}{2}}}\right] = \left[\frac{SHC^{\frac{1}{2}}}{SHC_{max}^{\frac{1}{2}}}\right] \quad [18]$$

$$\textbf{But}; \left[\frac{k^{\frac{1}{2}}}{k_{max}^{\frac{1}{2}}}\right] = \left[\frac{SHC^{\frac{1}{2}}}{SHC_{max}^{\frac{1}{2}}}\right] = \left[\frac{r}{r_{max}}\right] \quad [19]$$

Where r the pore radius in meter, rmax the maximum pore radius in meter, Take the logarithm of equation 19

$$\log\left[\frac{k^{\frac{1}{2}}}{k_{max}^{\frac{1}{2}}}\right] = \log\left[\frac{SHC^{\frac{1}{2}}}{SHC_{max}^{\frac{1}{2}}}\right] = \log\left[\frac{r}{r_{max}}\right] \quad [20]$$

$$\textbf{But}; \log\left[\frac{r}{r_{max}}\right] = \left[\frac{\log S_w}{3-Df}\right] \quad [21]$$

Insert equation 21 into equation 20

$$\log[SHC^{1/2} / SHC_{max}{}^{1/2}] = [\log S_W / 3 - DF] \qquad [22]$$

Equation 22 after log removal will become

$$S_w = \left[\frac{SHC^{\frac{1}{2}}}{SHC_{max}^{\frac{1}{2}}} \right]^{[3-Df]} \qquad [23]$$

Equation 23 the proof of equation 1 which relates the water saturation, specific heat capacity, maximum specific heat capacity and the fractal dimension. The capillary pressure can be scaled as

$$Sw = [Df - 3] * Pc * constant \qquad [24]$$

Where Sw the water saturation, Pc the capillary pressure and Df the fractal dimension.

Results and Discussion

Based on field observation the Shajara Reservoirs of the Permo-Carboniferous Shajara Formation were divided here into three units as described in Figure1. These units from bottom to top are: Lower Shajara Reservoir, Middle Shajara reservoir, and Upper Shajara Reservoir. Their attained results of the Specific heat capacity fractal dimension and capillary pressure fractal dimension are shown in Table 1. Based on the achieved results it was found that the Specific heat capacity fractal dimension is equal to the capillary pressure fractal dimension. The maximum value of the fractal dimension was found to be 2.7872 allocated to sample SJ13 from the Upper Shajara Reservoir as verified in Table 1. Whereas the minimum value of the fractal dimension 2.4379 was reported from sample SJ3 from the Lower Shajara reservoir as shown in Table1. The Specific heat capacity fractal dimension and capillary pressure fractal dimension were detected to increase with increasing permeability as proofed in Table1 owing to the possibility of having interconnected channels. Altogether, additional evidence to proof permeability increases with interconnected channels is the degree of sorting and friability.

Table 1: Petro physical model showing the three Shajara Reservoir Units with their corresponding values of Specific heat capacity fractal dimension and capillary pressure fractal dimension

Formation	Reservoir	Sample	Porosity %	K (md)	Grain size	Positive slope of the first procedure Slope=3-Df	Negative slope of the second procedure Slope=Df-3	Specific heat capacity fractal dimension	Capillary pressure fractal dimension
Permo-Carboniferous Shajara Formation	Upper Shajara Reservoir	SJ13	25	973	Coarse-grained	0.2128	-0.2128	2.7872	2.7872
		SJ12	28	1440	Very coarse grained	0.2141	-0.2141	2.7859	2.7859
		SJ11	36	1197	Medium-grained	0.2414	-0.2414	2.7586	2.7586
	Middle Shajara Reservoir	SJ9	31	1394	Medium-grained	0.2214	-0.2214	2.7786	2.7786
		SJ8	32	1344	Medium-grained	0.2248	-0.2248	2.7752	2.7752
		SJ7	35	1472	Coarse-grained	0.2317	-0.2317	2.7683	2.7683
	Lower Shajara Reservoir	SJ4	30	176	Coarse-grained	0.3157	-0.3157	2.6843	2.6843
		SJ3	34	56	Fine-grained	0.5621	-0.5621	2.4379	2.4379
		SJ2	35	1955	Medium-grained	0.2252	-0.2252	2.7748	2.7748
		SJ1	29	1680	Medium-grained	0.2141	-0.2141	2.7859	2.7859

The Lower Shajara reservoir was symbolized by six sandstone samples (Figure 1), four of which label as SJ1, SJ2, SJ3 and SJ4 were carefully chosen for capillary pressure measurement as proven in Table1. Their positive slopes of the first procedure log of the Specific heat capacity to maximum Specific heat capacity versus log wetting phase saturation (Sw) and negative slopes of the second procedure log capillary pressure (Pc) versus log wetting phase saturation (Sw) are clarified in Figure 2, Figure 3, Figure 4, Figure 5 and Table 1. Their Specific heat capacity fractal dimension and capillary pressure fractal dimension values are revealed in Table 1. As we proceed from sample SJ2 to SJ3 a pronounced reduction in permeability due to compaction was described from 1955 md to 56 md which reflects decrease in Specific heat capacity fractal dimension from 2.7748 to 2.4379 as quantified in table 1. Again, an increase in grain size and permeability was proved from sample SJ4 whose Specific heat capacity fractal dimension and capillary pressure fractal dimension was found to be 2.6843 as described in Table 1.

In contrast, the Middle Shajara reservoir which is separated from the Lower Shajara reservoir by an unconformity surface as revealed in Figure 1. It was nominated by four samples (Figure 1), three of which named as SJ7, SJ8, and SJ9 as illuminated in Table1 were chosen for capillary measurements as described in Table 1. Their positive slopes of the first procedure and negative slopes of the second procedure are shown in Figure 6, Figure 7

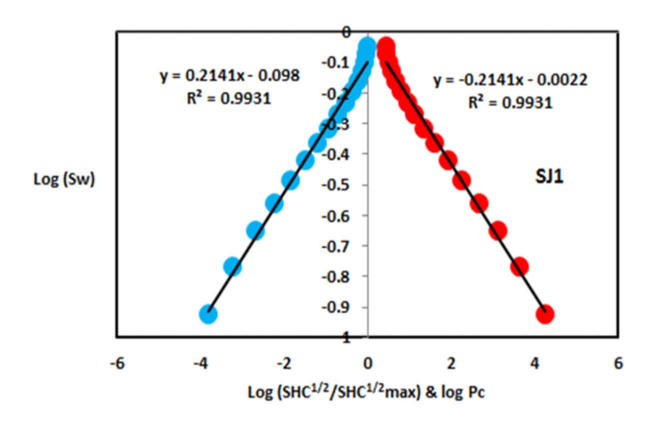

Figure 2: Log $(SHC^{1/2}/SHC^{1/2max})$ & log pc versus log Sw for sample SJ1

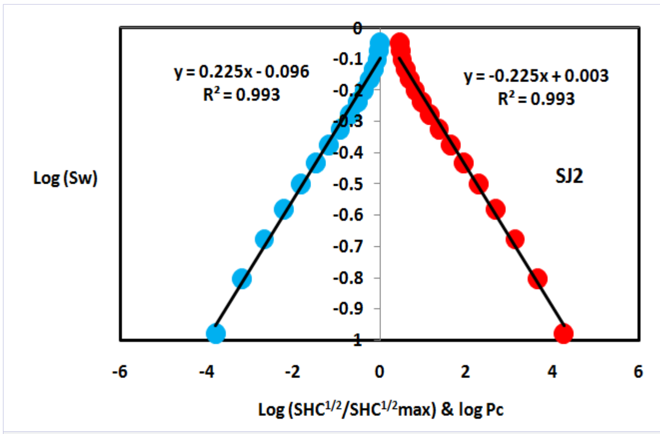

Figure 3: Log $(SHC^{1/2}/SHC^{1/2max})$ & log pc versus log Sw for sample SJ2

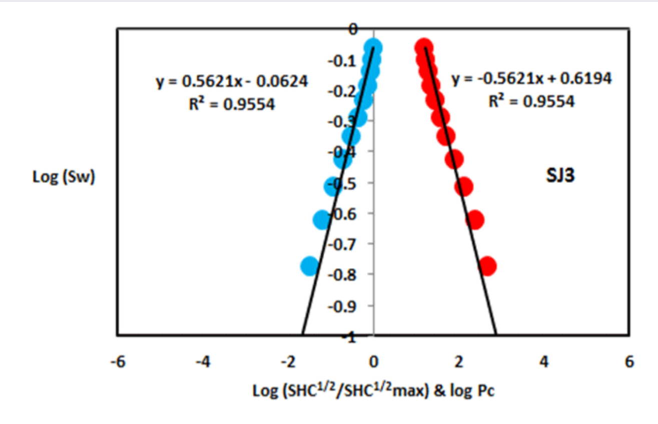

Figure 4: Log $(SHC^{1/2}/SHC^{1/2max})$ & log pc versus log Sw for sample SJ3

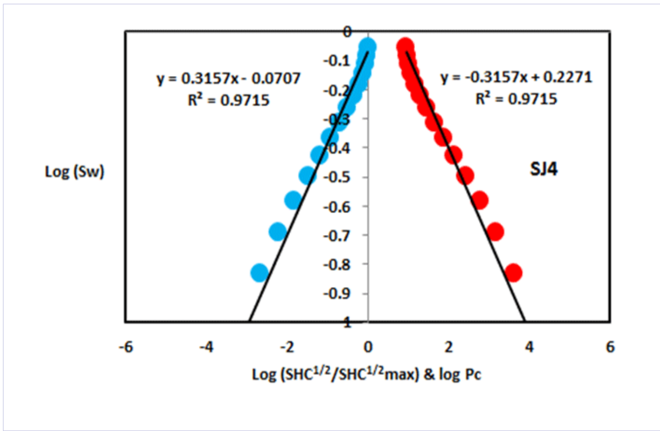

Figure 5: Log $(SHC^{1/2}/SHC^{1/2max})$ & log pc versus log Sw for sample SJ4

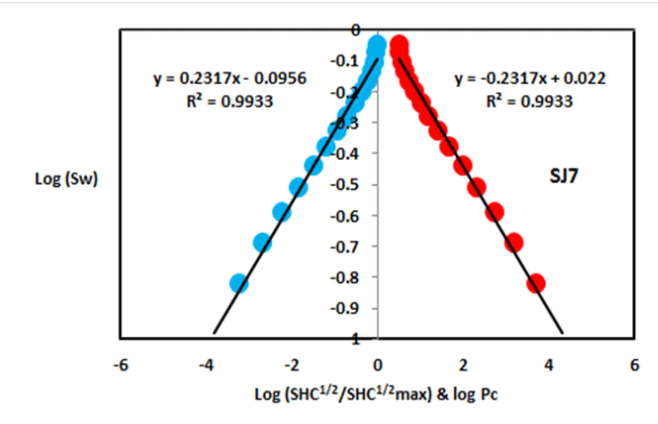

Figure 6: Log $(SHC^{1/2}/SHC^{1/2max})$ & log pc versus log Sw for sample SJ7

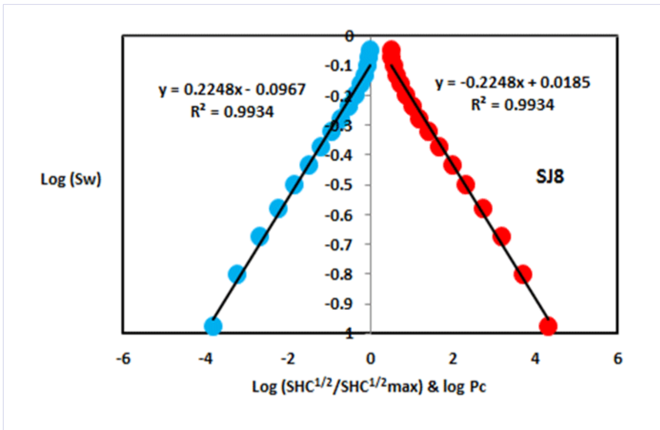

Figure 7: Log $(SHC^{1/2}/SHC^{1/2max})$ & log pc versus log Sw for sample SJ8

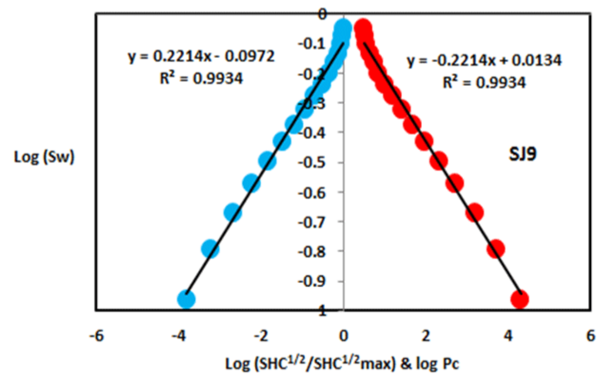

Figure 8: Log ($SHC^{1/2}/SHC^{1/2max}$) & log pc versus log Sw for sample SJ9

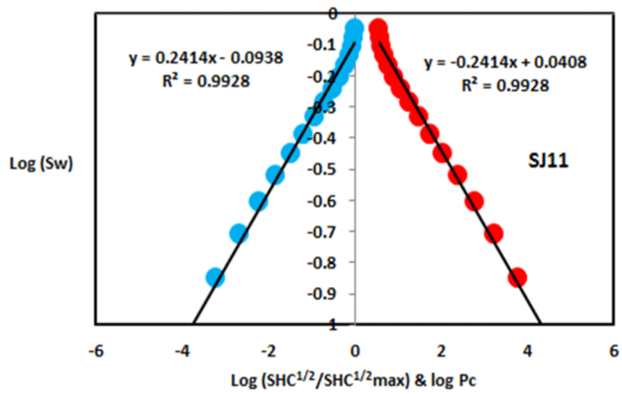

Figure 9: Log ($SHC^{1/2}/SHC^{1/2max}$) & log pc versus log Sw for sample SJ11

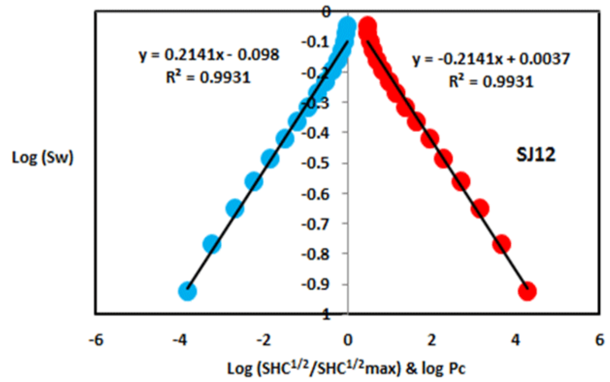

Figure 10: Log ($SHC^{1/2}/SHC^{1/2max}$) & log pc versus log Sw for sample SJ12

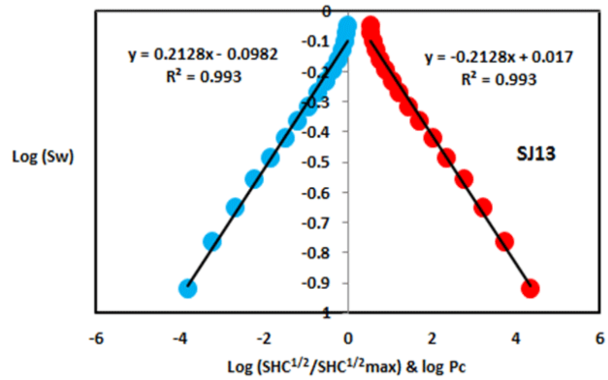

Figure 11: Log ($SHC^{1/2}/SHC^{1/2max}$) & log pc versus log Sw for sample SJ13

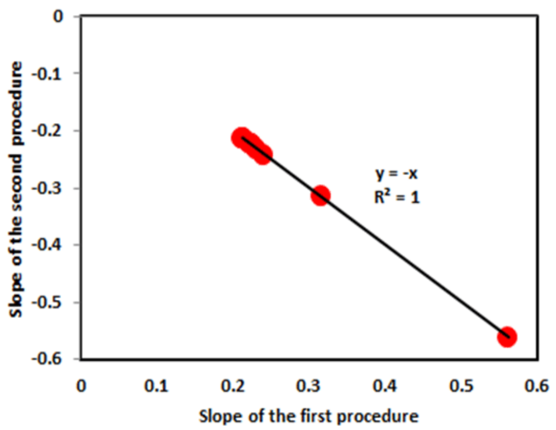

Figure 12: Slope of the first procedure versus slope of the second procedure

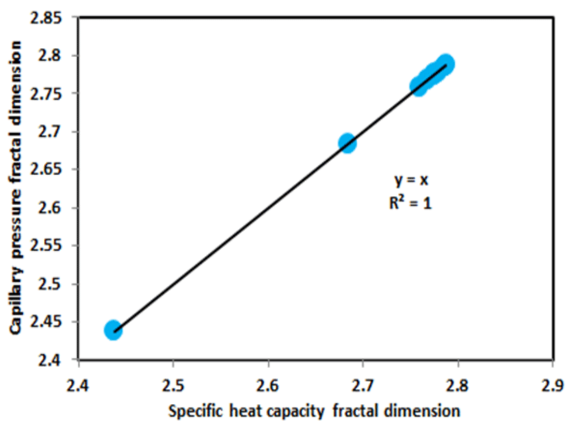

Figure 13: Specific heat capacity fractal dimension versus capillary pressure fractal dimension

and Figure 8 and Table 1. Furthermore, their Specific heat capacity fractal dimensions and capillary pressure fractal dimensions show similarities as defined in Table 1.Their fractal dimensions are higher than those of samples SJ3 and SJ4 from the Lower Shajara Reservoir due to an increase in their permeability as explained in table 1.

On the other hand, the Upper Shajara reservoir was separated from the Middle Shajara reservoir by yellow green mudstone as shown in Figure 1. It is defined by three samples so called SJ11, SJ12, and SJ13 as explained in Table 1. Their positive slopes of the first procedure and negative slopes of the second procedure are displayed in Figure 9, Figure 10 and Figure 11 and Table 1. Moreover, their Specific heat capacity fractal dimension and capillary pressure fractal dimension are also higher than those of sample SJ3 and SJ4 from the Lower Shajara Reservoir due to an increase in their permeability as simplified in table 1.

Overall a plot of positive slope of the first procedure versus negative slope of the second procedure as described in Figure 12 reveals three permeable zones of varying Petro physical properties. These reservoir zones were also confirmed by plotting Specific heat capacity fractal dimension versus capillary pressure fractal dimension as described in Figure 13. Such variation in fractal dimension can account for heterogeneity which is a key parameter in reservoir quality assessment.

Conclusion

The sandstones of the Shajara Reservoirs of the permo-Carboniferous Shajara Formation were divided here into three units based on Specific heat capacity fractal dimension. The Units from base to top are: Lower Shajara Specific Heat Capacity Fractal Dimension Unit, Middle Shajara Specific Heat Capacity Fractal Dimension Unit, and Upper Shajara Specific Heat Capacity Fractal Dimension Unit. These units were also proved by capillary pressure fractal dimension. As a whole, the fractal dimension was found to increase with increasing grain size, degree of sorting, friability, and permeability owing to possibility of having interconnected channels.

Acknowledgement

The author would to thank King Saud University, College of Engineering, Department of Petroleum and Natural Gas Engineering, Department of Chemical Engineering, Research Centre at College of Engineering, College of Science, Department of Geology and Geophysics, and King Abdullah Institute for research and Consulting Studies for their supports.

References

1. Frenkel J. On the theory of seismic and seismoelectric phenomena in a moist soil. Journal of physics.1944; 3(4):230-241.
2. Li K and Williams W. Determination of capillary pressure function from resistivity data. Transport in Porous Media. 2007; 67(1):1-15.
3. Revil A and Jardani A. Seismoelectric response of heavy oil reservoirs: theory and numerical modelling. Geophys J Int. 2010; 180(2):781-797. doi: 10.1111/j.1365-246X.2009.04439.x
4. Dukhin, A., Goetz, P., and Thommes M. Seismoelectric effect: a non-isochoric streaming current.1 Experiment. JColloid Interface Science.2010; 345(2): 547-553. doi: 10.1016/j.jcis.2010.02.010
5. Guan W., Hu H and Wang Z. Permeability inversion from low-frequency seismoelectric logs in fluid- saturated porous formations. Geophysical Prospecting. 2012; 61(1):120-133. doi: 10.1111/j.1365-2478.2012.01053.x
6. Hu H., Guan W., and Zhao W. Theoretical studies of permeability inversion from seismoelectric logs. Geophysical Research Abstracts 2012; 14: EGU2012-6725-1 2012 EGU General Assembly 2012.
7. Borde C., S´en´echal P, and Barri`ere J. etal., Impact of water saturation on seismoelectric transfer functions: a laboratory study of co-seismic phenomenon. Geophysical Journal International.2015; 200(3):1317-1335. doi: 10.1093/gji/ggu464
8. Jardani A. and Revil A. Seismoelectric couplings in a poroelastic material containing two immiscible fluid phases. Geophysical Journal International.2015; 202(2): 850-870. doi: 10.1093/gji/ggv176
9. Holzhauer J. Brito D., Bordes C. et al., Experimental quantification of the seismoelectric transfer function and its dependence on conductivity and saturation in loose sand. Geophysical Prospecting.2016;65:1097-1120.doi: 10.1111/1365-2478.12448
10. Peng R, Wei J-X., Di B-R etal., Experimental research on seismoelectric effects in sandstone. Applied Geophysics. 2016; 13(3):425-436.
11. Djuraev, U., Jufar, S.R., and Vasant. P. Numerical Study of frequency-dependent seismo electric coupling in partially-saturated porous media. MATEC Web of Conferences87, 02001(2017).1-6.doi: 10.1051/matecconf/20178702001
12. Alkhidir KEME. Pressure head fractal dimension for characterizing Shajara Reservoirs of the Shajara Formation of the Permo-Carboniferous Unayzah Group, Saudi Arabia. Archives of Petroleum and Environmental Biotechnology. 2017; 2:1-7. doi: 10.29011/2574-7614. 100113
13. Al-Khidir KE. On Similarity of Pressure Head and Bubble Pressure Fractal Dimensions for Characterizing Permo-Carboniferous Shajara Formation, Saudi Arabia. Journal of Industrial Pollution and Toxicity.2018;1(1):1-10.
14. Alkhidir KEME. Geometric relaxation time of induced polarization fractal dimension for characterizing Shajara Reservoirs of the Shajara Formation of the Permo-Carboniferous Unayzah Group, Saudi Arabia. Scifed Journal of Petroleum. 2018;2:1-6.
15. Alkhidir KEME. Geometric relaxation time of induced polarization fractal dimension for characterizing Shajara Reservoirs of the Shajara formation of the Permo-Carboniferous Unayzah Group-Permo. International Journal of Petrochemistry and Research. 2018;2:105-108.